# On the role of stereo-electronic effects in tuning the selectivity and rate of DNA alkylation by duocarmycins†

**Paola Cimino,[a,b] Giuseppe Bifulco,[b] Raffaele Riccio,[b] Luigi Gomez-Paloma[b] and Vincenzo Barone*[a]**

*Received 20th October 2005, Accepted 6th February 2006*
*First published as an Advance Article on the web 27th February 2006*
**DOI: 10.1039/b514890a**

The role of local geometric and stereo-electronic effects in tuning the alkylation of DNA by duocarmycins has been analyzed by an integrated computational tool rooted in the density functional theory and the polarizable continuum model. Our study points out that together with steric accessibility, different electronic delocalisations also contribute to determine the higher reactivity of adenine with respect to guanine. Also the effect of the methyl ester group on the alkylating agent has an electronic origin. Furthermore, deviations from the planarity in the drug structure (conformational catalysis) could be less important than currently accepted since, according to our computations, compounds with strongly different reactivity have nearly constant and very similar out of plane distortions before and after the reaction. Model computations suggest, instead, that specific non covalent interactions could discriminate between different drugs selectively reducing some activation energies with respect to the corresponding processes in solution.

## 1. Introduction

The search for new anticancer agents is an important area of research because current chemotherapy is still largely based on systemic delivery of drugs with poor selective cytotoxicities.

Many efforts are currently directed toward the discovery of anticancer agents able to bind directly to DNA or to inhibit DNA-binding enzymes.[1–4] In this framework, the interest in the DNA alkylating agents is expanding, as demonstrated by the recent synthesis and characterization of small molecules like ecteineascidin 743,[5] brostacillin,[6,7] pyrrolobenzodiazepines,[8,9] isofulven,[10] CC-1065 and duocarmycin analogs.[11–17]

(+)-Duocarmycin SA (DSA (**1**), Fig. 1), isolated from cultures of *Streptomyces*,[11] has revealed promising antitumor activity as a result of its capacity to bind within AT-rich minor groove regions of duplex B-DNA forming a covalent adduct (Fig. 2). Although the chemical pathway leading to the formation of the covalent adduct has not yet been fully elucidated, recent studies of structure–activity relationships provided interesting insights.

The DNA alkylation reaction by (+)-DSA and its derivatives is exceptionally facile and proceeds *via* a nucleophilic attack of an adenine (N3) to the least substituted carbon of the cyclopropyl group.[11] This efficient alkylation of DNA is in contrast with the high stability of these molecules under solvolytic conditions.[18–21] Furthermore, the strong experimental evidence that the alkylation of DNA by duocarmycin does not require acid catalysis[22–24] points out the role of a DNA binding-induced conformational change[25,26] able to reduce the vinylogous amide conjugation in the alkylation subunit with the consequent activation of the ligands toward a nucleophilic attack. On these grounds, it has been suggested that the enhancement of the alkylating properties of duocarmycins by DNA is related to the lifting of the intrinsic near-coplanarity of the two subunits A and B (described by the torsion angles $\chi_1$, $\chi_2$, $\chi_3$, Fig. 1) induced by binding to AT-rich duplex DNA, with the consequent strong reduction of the conjugation present in the free ligand, and increase of the electrophilicity of the cyclopropyl ring. This effect could be sufficient to activate a nucleophilic addition independent of pH, under physiological conditions.

According to this model, the reaction rate would be related to the inter-subunit twist, namely a direct result of the structural features of the ligand. However, although the results of several experimental studies point out the importance of the methyl ester[27] on the alkylating unit A of duocarmycin SA and of the methoxy groups[28,29] on the binding unit B, the specific role of these substituents is still ill defined. In our opinion, a deeper insight into this problem can be obtained in terms of the reaction profile of model systems with special reference to the geometries and energies of prototype transition states. A quantum mechanical study could be the most appropriate tool to obtain such information, provided that the computational model couples reliability and feasibility for quite large systems.

Thanks to the recent advances in quantum mechanical (QM) methods rooted in the density functional theory (DFT)[30–32] and of continuum solvent models (*e.g.* the so called polarizable continuum model, PCM[32]), systems of biological and pharmacological interest in their natural aqueous environment can be nowadays treated with remarkable accuracy, a particularly effective approach being offered by hybrid functionals (here PBE0[33]) coupled to PCM.[32]

Using this integrated computational strategy, the first part of our study is devoted to the analysis of the electronic factors responsible for the selectivity of the (+)-DSA attack toward adenine through a comparative investigation of adenine and

[a]*Dipartimento di Chimica, Università Federico II, Complesso Universitario Monte S. Angelo, via Cintia, I-80126, Napoli, Italy. E-mail: baronev@unina.it*
[b]*Dipartimento di Scienze Farmaceutiche, Università di Salerno, via Ponte don Melillo, 84084, Fisciano (SA), Italy*

† Electronic supplementary information (ESI) available: Tables SI-1, SI-2, SI-3, SI-4, SI-5 and SI-6; Fig. SI-1, Fig. SI-2 and Fig. SI-3; *Z*-matrices, computed energies, imaginary frequencies and thermodynamic data for all optimized structures. See DOI: 10.1039/b514890a

 

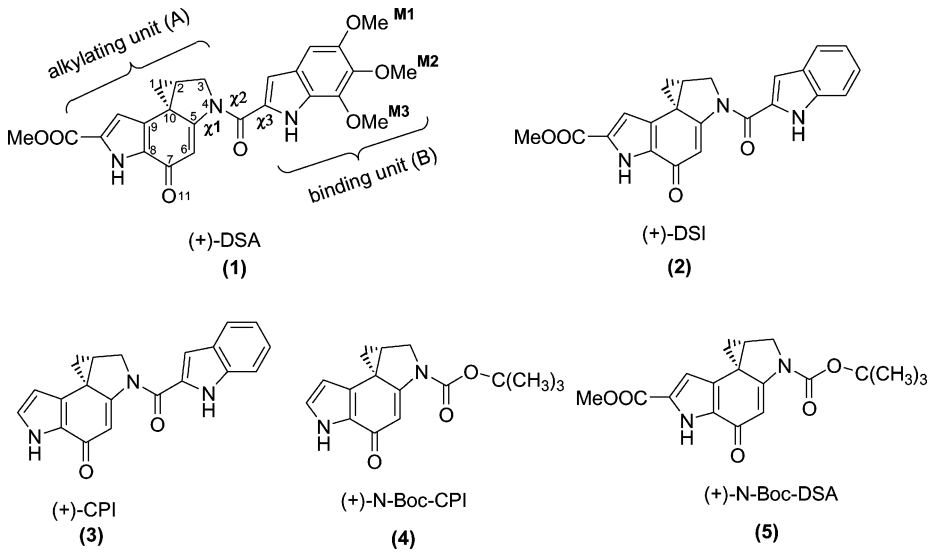


**Fig. 1** Structure of natural compound (+)-DSA (**1**), and synthetic compounds (+)-DSI (**2**), (+)-CPI (**3**), (+)-*N*-Boc-CPI (**4**), (+)-*N*-Boc-DSA (**5**).

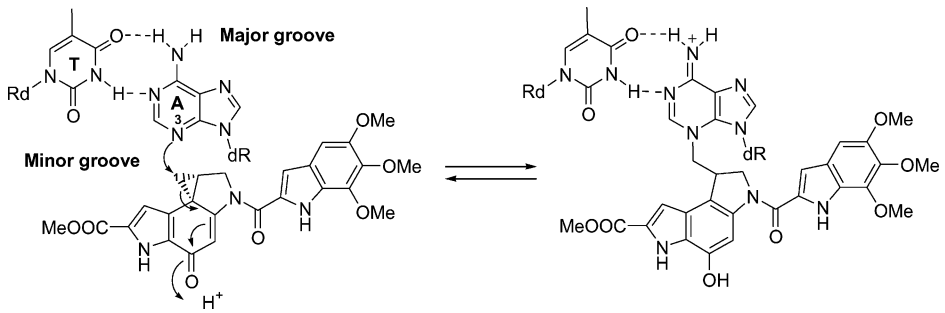


**Fig. 2** Schematic representation of the DNA alkylation.

guanine alkylation reactions, and to the evaluation of the role played by non covalent interactions on the title reaction. Next, we perform a comparative examination of representative models [(+)-DSI and (+)-CPI with adenine] allowing a detailed examination of the subunit A of the natural product, (+)-DSA. The side-by-side comparisons of the systems pointed out the role of electronic effects related to the presence of the methyl ester in influencing the overall reactivity and the most important structural features tuning the alkylation reaction. Furthermore, we present a preliminary exploration of the role of the methoxy groups on the binding unit (B), in terms of electronic effects, by a combined discrete–continuum model in which some specific interactions are modeled at the quantum mechanical level, whereas the effect of more distant parts of DNA is taken into account by means of an effective polarizable continuum. Finally, we tried to analyze reactivity trends in terms of hardness ($\eta$) and electrophilicity ($\omega$) indexes, obtained by DFT calculations.

The paper is organized as follows: in section 2, we describe the computational details of the methods used. Section 3 starts with the results obtained on the same ligand structures that have previously been analyzed experimentally, in order to assess the accuracy of the selected computational approach. Next, in subsection 3.1 we study the reaction of the same electrophilic species [(+)-CPI] with adenine and guanine; in subsection 3.2 we investigate the reaction with a simplified model analyzing the influence of the solvent and of hydrogen bonds, by using explicit water molecules; in subsection 3.3 we compare the reactivity of several ligands toward the same nucleophile (adenine). In section 4 we discuss our results in terms of the different factors possibly influencing the reactivity, and we end with conclusions.

## 2. Methods

### 2. Computational details

All the calculations were carried out using the Gaussian03 package.[34] In the gas phase, all structures were fully optimized and characterized as minima or transition states by calculating the harmonic vibrational frequencies at the PBE0/6-31G(d) level.[33–35] Zero point energies (ZPE's) and thermal contributions to thermodynamic functions and activation parameters were computed from PBE0/6-31G(d) structures and harmonic frequencies by using the rigid rotor–harmonic oscillator approximation and the standard expressions for an ideal gas in the canonical ensemble at 298.15 K and 1 atm.

Solvent effects have been taken into account by PCM,[32] in which the solvent is represented by an infinite dielectric medium characterized by the relative dielectric constant of the bulk. We recall that the solvation energies obtained from PCM computations have the status of free energies, since they implicitly take into account the thermal and entropic contributions of the solvent.[36]

Reaction paths were characterized at the PBE0/6-31G(d) level in terms of the intrinsic reaction coordinate (IRC)[37] starting from the optimized transition structure (TS) and using 10 steps in each direction, with a step size of 0.3 $amu^{-1/2}$ bohr.

Electronic structures were then analyzed using the natural bond orbital (NBO) model, which allows evaluation of the stabilization energy connected to interactions between occupied orbitals of one reactant and empty orbitals of the second one.[38]

Finally, we have computed some reactivity indexes quantifying both the overall reactivity and the site selectivity of a molecule. We have selected as global descriptors the electrophilicity $\omega$ (an intramolecular parameter that depends only on the electronic characteristics of the acceptor species)[39] and the donor–acceptor hardness $\eta_{DA}$ (an intermolecular parameter).[40]

The hardness has been defined[41–43] as the difference between the vertical ionization energy ($I$) and the electron affinity ($A$) of the neutral molecule, $\eta = I - A$ where: $I = E(N = N_0 - 1) - E(N = N_0)$ and $A = E(N = N_0) - E(N = N_0 + 1)$, $N_0$ being the number of electrons in the ground state of the system. This requires the calculation of the energies of the neutral ($N_0$ electron system), cationic ($N_0 - 1$ electron system), and anionic ($N_0 + 1$ electron system) forms of each system. Note that the reliability of the PBE0 functional in the computation of I's and A's has been checked before,[33] and that we have used unrestricted Hamiltonians for open shell species. The electronegativity ($\chi$) and the electronic chemical potential ($\mu$) have been defined as: $\chi = (I + A)/2 = -\mu$. The definition of the electrophilicity index ($\omega$), given by Parr and Pearson[39] is: $\omega = \mu^2/2\eta$. Finally, the donor–acceptor intermolecular hardness ($\eta_{DA}$) is $\eta_{DA} = (I_D - A_A)$, where $A_A$ is the electron affinity of the acceptor A and $I_D$ is the vertical ionization energy of the donor molecule D.[40]

## 3. Results and discussion

Before analyzing our computational results, it is useful to summarize the most significant information on the title reaction obtained in previous studies.

The available experimental data include the X-ray structures of DSA derivatives,[44,45] several high resolution NMR structures[46–49] of ligand–DNA complexes, and a wealth of data regarding the relative alkylation rates[45] of synthetic DSA derivatives (Tables 1, 2). We point out that the X-ray structure of a DSA derivative (*N*-Boc-CPI, **4**, Fig. 1), that has a *tert*-butyloxy group instead of the binding subunit, corresponds closely to the predicted conformation of the free ligand in solution with coplanar arrangements of the two subunits (Table 2).

**Table 1** Torsional angles ($\chi_1$, $\chi_2$ and $\chi_3$) for the covalent adducts with (+)-DSA (**1**), (+)-DSI (**2**) and (+)-CPI (**3**). Reactivity for (+)-DSA, (+)-DSI and (+)-CPI in the presence of DNA

| | Dihedral angles | | |
|---|---|---|---|
| NMR data (DNA–ligand complex) | $\chi_1$ | $\chi_2$ | $\chi_3$ |
| **1** | 22.4 | 11.0 | 11.4 |
| **2** | 14.2 | 13.4 | 9.7 |
| **3** | 14.2 | 14.7 | 8.8 |
| Relative rates of DNA alkylation[a] | $K_{rel}$ | | |
| **1** | 1.000 | | |
| **2** | 0.050 | | |
| **3** | 0.004 | | |

[a] At the w794 high affinity site 5′-AATTA.

**Table 2** Experimental and calculated torsional angles ($\chi_1$and $\chi_2$) for the free ligand (+)-*N*-Boc-CPI (**4**). The structure has been optimized for the gas phase [PBE0/6-31G(d)] and for an aqueous solution [PCM–PBE0/6-31G(d)]

| | Dihedral angles | |
|---|---|---|
| Conditions | $\chi_1$ | $\chi_2$ |
| Exp./X-ray | 12.6 | 6.3 |
| QM/gas phase | 11.4 | 7.1 |
| QM/aqueous solution | 12.8 | 7.2 |

The structurally characterized covalent complexes have been obtained with three of the different ligands shown in Fig. 1: the natural compound (+)-DSA (**1**) and two synthetic simplified analogues, (+)-DSI (**2**) and (+)-CPI (**3**). Note that both synthetic models do not bear any methoxy group on the binding subunit (B), and that **3** also lacks the acetyl group on the alkylating subunit (A). In all the ligand–DNA complexes characterized until now the alkylated product shows a covalent bond between the nitrogen (adenine N3) and the least substituted cyclopropyl carbon atom (C1), a phenolic system developed from the dienone present in the initial structure of the ligand and a distorted conformation due to a twist between the two planar subunits.

In our previous computational studies,[50,51] where a variety of (+)-DSA derivatives with several nucleophiles have been used as models for the alkylation in acid and neutral conditions, we showed that, in agreement with the experimental evidence,[11] the reaction proceeds through an $S_N2$ mechanism, with the nucleophilic attack at the least substituted carbon atom of the cyclopropane moiety. In all molecules the driving force of the reaction is the development of an aromatic system (Scheme 1).

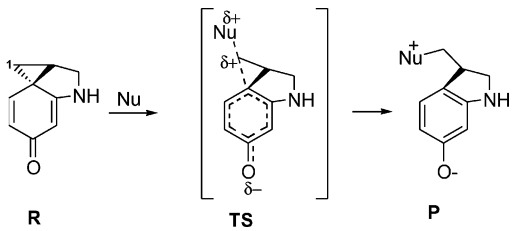


**Scheme 1** Schematic pathway for the $S_N2$ reaction, under neutral conditions.

Taking into account the results of several experimental studies, we decided to investigate the attack of DNA bases on the neutral form of the ligands assuming that the proton transfer to the oxygen anion formed in the product **P** (Scheme 1) is a fast process, and that the rate determining step is the nucleophilic attack on the cyclopropylic carbon atom (C1).

We have modeled the alkylation reaction of DNA with duocarmycins using compounds **1**, **2** and **3** (Fig. 1), and adenine as nucleophiles since, as mentioned above, experimental structures are available for the final DNA–ligand complexes (Table 1).

Before that, however, we have optimized the structure of the experimentally characterized free ligand **4**. The good agreement

 

**Table 3** Activation energies in kcal mol$^{-1}$ (298.15 K, 1 atm) for compounds **1**, **2** and **3** with adenine calculated for the gas phase with different functionals and with basis set 6–31G(d)

| | Compound | | |
|---|---|---|---|
| $\Delta E^{\ddagger}$ (gas phase) | **1** | **2** | **3** |
| PBE0 | 30.9 | 29.8 | 31.1 |
| PBE | 23.8 | 22.4 | 23.6 |
| BLYP | 26.8 | 25.8 | 27.1 |

between the computed and experimental geometric parameters (Table 2) provides a convincing validation of our computational approach for this class of compounds. Next, the level of theory required to accurately describe the energetics of the studied processes has been assessed by computing the energy barrier governing the reaction of compounds **1**, **2** and **3**, at various levels. The results in Table 3 show that the activation energy calculated with a hybrid functional (PBE0) is higher than with conventional functionals (PBE, BLYP), but the reactivity trends are always the same. Since previous studies for smaller models[50,51] showed that MP2 and PBE0 results are very similar, and that basis set extension above the 6-31G(d) level has a negligible effect, in the following we will discuss only PBE0/6-31G(d) results. In the same studies[50,51] we have evaluated the bare energy $\Delta E^{\ddagger}$ (*i.e.* the electronic energy differences between transition states and reactants), together with the corresponding free energies ($\Delta G^{\ddagger}$), which include zero-point, thermal, and entropic contributions. Since we always found that $\Delta E^{\ddagger}$ and $\Delta G^{\ddagger}$ have parallel trends ($\Delta G^{\ddagger} > \Delta E^{\ddagger}$ by about 10 kcal mol$^{-1}$), in the present paper, dealing with significantly larger systems, we decided to discuss the $\Delta E^{\ddagger}$'s only. This hypothesis is, of course, acceptable only for reactions with similar molecularity as is the case for all processes investigated in the following sections.

The structural parameters of the optimized structures are presented in Tables 1, 2, 7, 8, 10, SI-1, SI-2, SI-3, SI-4, SI-5 and SI-6†; the energies are reported in Tables 3, 4, 5, 6 and 9.

In order to investigate if environmental effects could modify geometric parameters in a significant way we optimized structure **4** in a continuum of uniform dielectric constant ($\varepsilon = 78.0$), using the PCM,[32] that represents bulk effects well. Our results confirm that the environment does not induce significant geometrical changes in the systems and that energetic parameters obtained employing structures optimized *in vacuo* are very close to their counterparts issuing from geometry relaxation in the polarizable continuum.[31,36,51] Since geometry optimizations in PCM are quite cumbersome, we decided on the grounds of the above results to evaluate the environmental effects for the larger systems by single-point PCM calculations at geometries optimized in the gas phase.

### 3.1 Comparison between adenine and guanine

One of the crucial points to define the characteristics of the DNA alkylation reactions is the determination of the origin of the AT-rich alkylation selectivity. Although experimental studies defined a number of key features that contribute to the sequence-selective DNA alkylation by members of this class of agents, the selectivity for the almost exclusive addition to adenine remains an open question. The only hypothesis put forward until now is that the nucleophilic addition occurs at the most accessible of the two most nucleophilic sites in the minor groove (adenine N3 *versus* guanine N3).[11] Here, we will investigate if intrinsic electronic effects could play any role in determining the selectivity by using the model compound **3** (CPI, Fig. 1). We will consider only purinic bases (adenine and guanine) since the other two DNA bases (cytosine and thymine) are not able to attack an electrophilic species. Our results show that the reaction follows the same $S_N2$ mechanism discussed above. Examination of the calculated reaction and activation energies shows that in the gas phase all the processes are endothermic and that the energy barrier ($\Delta E^{\ddagger}$) governing the alkylation reaction of **3** with guanine is higher than with adenine by about 8 kcal mol$^{-1}$ (Table 4). The product structures are characterized by an aromatic moiety with the C1–C10 bond nearly coplanar to the ring. Most of the features of the transition state with guanine (TS-guanine) do not differ significantly from that with adenine (TS-adenine) (Fig. 3, SI-1, SI-2†). Indeed, in both structures the developing aromaticity is evidenced by the bond lengths and the dihedral angles $\alpha$ (C6–C5–C10–C2), $\beta$ (C6–C5–C10–C1), $\gamma$ (C6–C5–C10–C9) and $\delta$ (C8–C9–C10–C5), with the C2–C10 bond going to become coplanar to the ring, while the C1–C10 bond shifts toward a more perpendicular arrangement. However, there are some differences related to different reactivities. Fig. 3 shows that the length of the incipient bond (C1–nitrogen) differs appreciably between the reactions, and this difference is a remarkable feature of both transition states (Fig. 3). Indeed, the

**Table 4** Activation energy in kcal mol$^{-1}$ (298.15 K, 1 atm) in the gas phase [PBE0/6-31G(d)] for the reaction of the compound **3** with adenine and guanine

| Gas phase | Adenine | Guanine |
|---|---|---|
| $\Delta E^{\ddagger}$ (TS–reactants) | 31.1 | 38.8 |
| $\Delta E$ (product–reactants) | 19.8 | 28.1 |

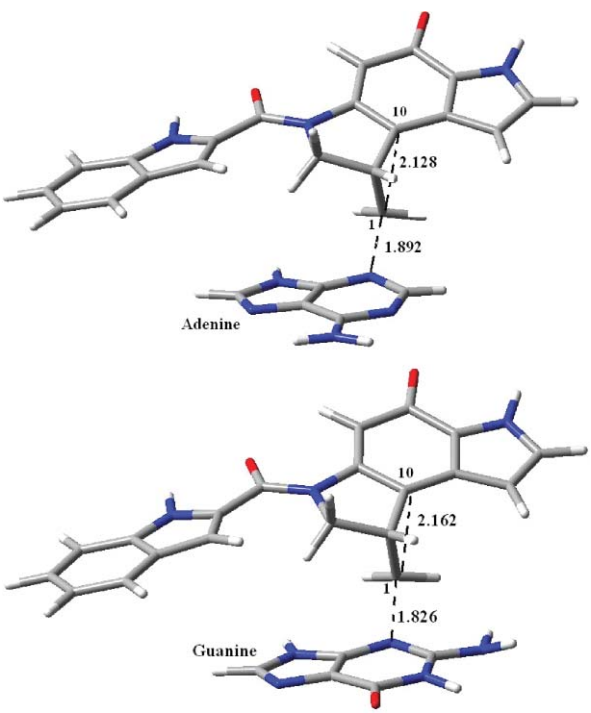


**Fig. 3** Structure of the transition state (**TS-3**) of (+)-CPI with DNA bases optimized at PBE0/6-31G(d) level. The bond lengths are in Angstroms.

C1–nitrogen bond in TS-adenine is longer (1.892 Å) than that in TS-guanine (1.826 Å), and this could be a consequence of a greater facility of adenine to react. This is in agreement with Hammond's postulate[52] which predicts a transition state with a structure closer to that of the product for the reaction with guanine and a transition state more resembling the reactants for adenine (see Tables SI-1, SI-2†).

The analysis of the transition states is completed by the NBO analysis, the results of which are summarized in Tables SI-4 and SI-5.† Indeed, the hybridization of the atoms in the TSs (Table SI-4) shows that TS-adenine still presents the C1–C10 bond, whereas in TS-guanine the C1–C10 bond is already broken and the lone pair on the nucleophile has almost become the σ bond between the carbon C1 and the nitrogen. These data are indicative of an "early" TS structure for adenine (closer to the reactants) and of a "late" TS for guanine (closer to the product). The most significant stabilizing interactions governing the reaction with adenine involve the C1–C10 bond (σ*) and the LP orbital of the adenine nitrogen (98.1 kcal mol$^{-1}$, Table SI-5). This confirms the prominent role of the nitrogen lone pair of adenine in stabilizing a TS with a structure quite close to that of the reactants, with a consequent lower activation energy.

Thus, the stabilizing interactions operative for the adenine and guanine nitrogens are slightly different, possibly due to different electron delocalization in the base rings leading, *inter alia*, to a greater electronic occupancy of the nitrogen LP orbital in adenine than in guanine (Table SI-6†). It is noteworthy that adenine is characterized by a canonical aromatic system (N1–C2–N3–C4–C5–C6), whereas in the guanine the presence of the carbonyl group induces the formation of a C2–N3–C4–C5–C6–O10 π-system, with an increased double bond character for the C2–N3 bond and a reduction of the electronic density on the nucleophilic nitrogen.

### 3.2 Influence of environmental and specific interactions on the reaction rate

A quantitative investigation of the role of more distant parts of DNA in tuning the reaction would possibly require a dynamical approach.[53] Here, however, we are more interested in general trends, which could be obscured by the specific details of different simulations for different drugs. As a consequence we resorted to a simpler model in which non specific effects are described in terms of a continuum polarizable medium with a dielectric constant typical of biological systems ($2 < \varepsilon < 8$).[54] Next, specific effects are considered enlarging the system treated at the quantum mechanical level by models including the local environment of DNA fragments showing short contacts with the reacting moiety (DSA, DSI or CPI). We recall that, for non overlapping systems, the electrostatic potential (and/or electric field) experienced by a fragment can be expressed exactly in terms of apparent charges spread on a suitable separating surface. Of course, here we make the further assumption that the differential effect of the DNA field on reactants and transition states is well reproduced by the combined contributions of the small fragments treated explicitly and of the continuous polarizable medium mimicking long range effects. A number of studies are showing that, under favorable conditions, this approach can provide realistic trends without the need of knowing the precise structural characteristics of large biological systems at an atomic resolution.[55]

On this basis we will examine first the effect of intermolecular hydrogen bonds with the carbonyl moiety present in all ligands; next, we will focus our attention on the effects of this kind of interaction on the methoxy groups of (+)-DSA. In both cases, for purposes of illustration, additional non specific environmental effects will be taken into account by means of polarizable continuum media with dielectric constants ($\varepsilon$) ranging between 4 and 8 which corresponds to the accepted range of the effective dielectric constant in biological systems. In some cases, a dielectric constant of 78 (bulk water) was also considered.

The study of the quite complex models discussed in this paper requires considerable computer resources. To simplify matters we considered at first the reaction between a (+)-DSA derivative, (+)-*N*-Boc-CPI (**4**) and pyridine. The results in Table 5 show that the activation energies for the reaction of (+)-CPI with adenine and pyridine are very close and that the two models, (+)-CPI and (+)-*N*-Boc-CPI give comparable results. These data suggest that the chosen model may be adequate for determining reliable relative energies.

Table 6 shows that the activation energies of the reaction in solution between compound **4** with pyridine are smaller than in the gas phase and that the energies decrease when the dielectric constant of the medium is increased. In particular, in aqueous solution our computations predict that the barrier for the reaction is significantly lower than in the gas phase and this can be related to the stabilization of the structures involving charge separation by polar solvents.

Next, keeping in mind that in the alkylation reaction a water molecule could act as a proton relay, one or two water molecules can be involved in relatively strong hydrogen bonds linking the reactants. In our model (Fig. 4), when one water molecule is hydrogen bonded to the carbonylic oxygen in **4**, the barrier height of the transition state (**TS-4S**) is reduced to 30.2 kcal mol$^{-1}$. If two molecules of water are hydrogen bonded, the barrier further decreases to 28.3 kcal mol$^{-1}$. Although entropy effects can, of course, modify the quantitative results, we think that the general

**Table 5** Activation energy in kcal mol$^{-1}$ (298.15 K, 1 atm) for the reaction of the compound **3** (CPI) and **4** (*N*-Boc-CPI) with adenine (gas phase) and pyridine (both gas phase and aqueous solution)

| Nucleophile | **3** | **4** |
|---|---|---|
| *Gas phase* | | |
| Pyridine | 31.0 | 32.4 |
| Adenine | 31.1 | — |
| *Aqueous solution* | | |
| Pyridine | 21.3 | 22.5 |

**Table 6** Activation energy in kcal mol$^{-1}$ (298.15 K, 1 atm) in the gas phase [PBE0/6-31G(d)] and in aqueous solution [PCM–PBE0/6-31G(d)] for the reaction between compound **4** and pyridine with one (**S**) and two (**2S**) solvent molecules

| | **4** | **4** + **S** | **4** + **2S** |
|---|---|---|---|
| $\Delta E^{\ddagger}$ (gas phase) | 32.4 | 30.2 | 28.3 |
| $\Delta E^{\ddagger}$ ($\varepsilon = 4.0$) | 27.0 | 24.5 | 22.5 |
| $\Delta E^{\ddagger}$ ($\varepsilon = 8.0$) | 25.5 | 23.0 | 21.1 |
| $\Delta E^{\ddagger}$ ($\varepsilon = 78.0$) | 22.5 | 20.0 | 18.0 |

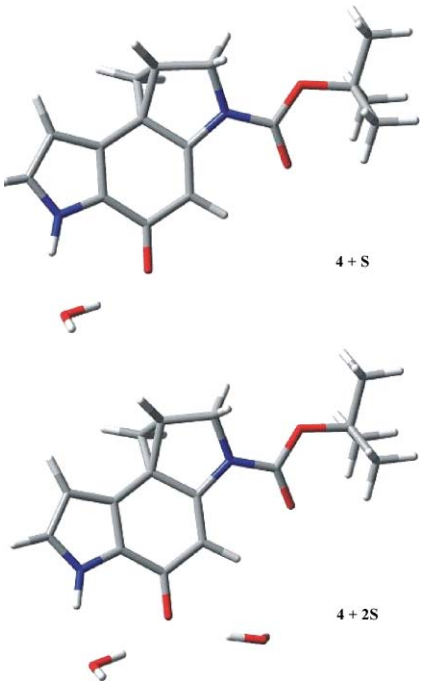


**Fig. 4** Structure of the (+)-*N*-Boc-CPI with one (**S**) and two (**2S**) water molecules optimized at PBE0/6-31G(d) level.

**Table 7** Torsional angles ($\chi_1$, $\chi_2$) for the free ligand **4** optimized for the gas phase [PBE0/6-31G(d)] with one (**S**) and two (**2S**) solvent molecules

| | Dihedral angles | |
|---|---|---|
| Reactants | $\chi_1$ | $\chi_2$ |
| **4** | 11.4 | 7.1 |
| **4** + **S** | 10.8 | 6.7 |
| **4** + **2S** | 14.3 | 8.0 |

trend suggested by the $\Delta E^{\ddagger}$'s remains significant. From another point of view, Table 7 shows that the structural changes induced by the presence of explicit water molecules are quite small.

These results support the idea that the reactivity of the (+)-DSA derivatives can be influenced by the number and type of hydrogen bonding interactions with the solvent and/or with other parts of the DNA. We will try to take into account both short- and long-range effects by adding some explicit fragments to simulate local interactions with the reacting system and then embedding the whole system in a dielectric continuum mimicking non specific interactions with more distant parts of the biological substrate (see Table 6). It is noteworthy that in most cases the effect of both contributions is nearly additive.[55]

### 3.3 Effect of substituents on the alkylating and binding units

**3.3.1 The methyl ester group on the alkylating unit.** We recall that there is a general consensus about the leading catalytic effect of a "binding-induced conformational change" in the alkylating agent. However, there are different points of view concerning how the torsion between the two subunits can be connected to the alkylation rate. On the one hand, the observed inter-subunit twist angle values in the end products ($\chi_1$, $\chi_2$ and $\chi_3$, Table 1) of (+)-DSA and (+)-DSI correlate with the reaction rates, suggesting that larger torsions could lead to faster DNA alkylation (DSA > DSI). Indeed, the comparison of the 3D structure of the (+)-DSA–DNA adduct with that of the (+)-DSI–DNA adduct reveals differences in the torsion angles, and, on the basis of the reaction rates (DSA > DSI), supports the idea that the absence of the methoxy groups on the binding subunit reduces the reaction rate and that there is a correlation with the torsion angle (DSA > DSI).

On the other hand, the significantly greater alkylation rate of (+)-DSI with respect to (+)-CPI (about 10 times) should imply quite different inter-subunit twists in the bound conformation of the two ligands, which are, on the contrary, very similar (see Table 8). Thus, it is quite clear that the inter-subunit twist cannot be the only factor influencing the reactivity and/or that the methyl ester on the alkylating subunit has a direct effect in tuning the alkylation efficiency of these agents.

Let us now investigate the role of the methyl ester on the alkylating subunit in determining the reactivity beyond its mere ability to increase the rigid length of the molecule. We start our analysis by characterizing the structure of the free ligands, (+)-DSA, (+)-DSI and (+)-CPI (**1**, **2** and **3**, Fig. 5), and of the end products (**P-1**, **P-2** and **P-3**, Table SI-3†). The structural investigation of **1**, **2** and **3** shows that the most stable conformation for the reactants, fully optimized for the gas phase, already presents a quite large inter-subunit twist, with $\chi_1$, $\chi_2$ and $\chi_3 \approx 19°$, 7° and 8°, respectively. As shown in Table 8, the values of these three dihedral angles are similar also in the structures optimized for an aqueous solution. As a matter of fact, the optimization of the ligand

**Table 8** Torsional angles ($\chi_1$, $\chi_2$ and $\chi_3$) for the free ligands optimized for the gas phase [PBE0/6-31G(d)] and for an aqueous solution [PCM–PBE0/6-31G(d)], and for the transition state structures and the products optimized for the gas phase [PBE0/6-31G(d)]

| | Dihedral angles | | |
|---|---|---|---|
| Reactants | $\chi_1$ | $\chi_2$ | $\chi_3$ |
| Gas phase | | | |
| **1** | 19.0 | 7.8 | 8.4 |
| **2** | 18.5 | 7.7 | 7.7 |
| **3** | 18.8 | 7.4 | 7.7 |
| Aqueous solution | | | |
| **1** | 21.8 | 8.2 | 11.4 |
| **2** | 22.5 | 8.1 | 12.1 |
| **3** | 23.4 | 7.7 | 12.7 |
| Transition states | $\chi_1$ | $\chi_2$ | $\chi_3$ |
| Gas phase | | | |
| **1**–Adenine | 27.5 | −4.7 | 14.4 |
| **2**–Adenine | 26.6 | −4.6 | 14.6 |
| **3**–Adenine | 26.1 | −4.3 | 14.0 |
| Products | $\chi_1$ | $\chi_2$ | $\chi_3$ |
| Gas phase | | | |
| **P-1**–Adenine | 31.9 | −4.1 | 26.4 |
| **P-2**–Adenine | 23.4 | −4.0 | 15.8 |
| **P-3**–Adenine | 23.2 | −3.4 | 16.2 |

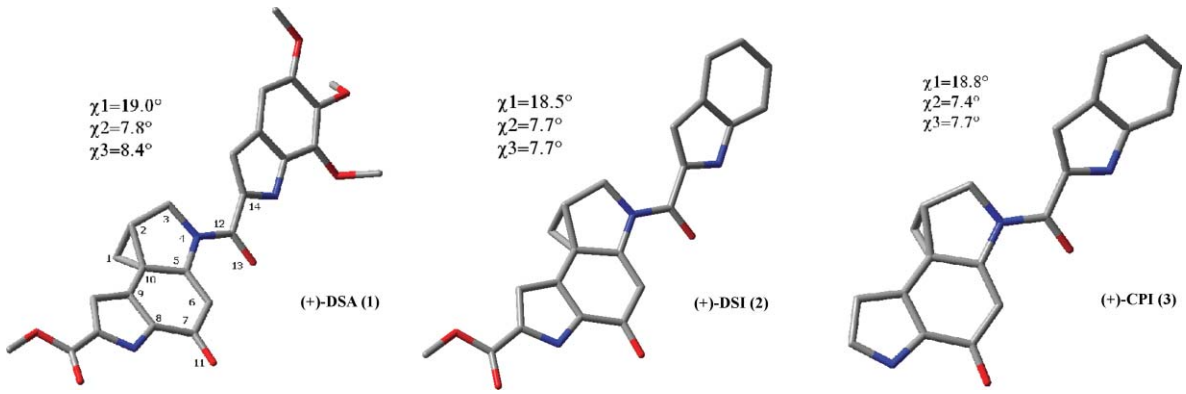


**Fig. 5** Structure of compounds **1**, **2**, and **3** optimized at the PBE0/6-31G(d) level.

(**1** and **3**) for the gas phase while gradually changing the dihedral angle $\chi_1$ by 5° steps (0°, 5°, 10°, 15°, 20°, 25°, 30°) shows that the resulting structures are only slightly different concerning both geometry and energy (Fig. SI-2†), in agreement with a previous study.[56] In particular, distortion of $\chi_1$ from 0° to 20° leads to an energy change of just 0.6 kcal mol$^{-1}$.

An analysis of the geometry of the optimized structures (Tables SI-1 and SI-3†) shows in all products (**P-1**, **P-2** and **P-3**) the same system characterized by an aromatic moiety with the C1–C10 bond nearly coplanar to the ring and a distorted conformation with quite large $\chi_1$ torsion angles (31.0°, 23.4° and 23.2° for **P-1**, **P-2** and **P-3**, respectively, see Table 8).

In summary, the free ligands show similar twisted conformations (Fig. 5), whereas the DSA–adenine adduct is the most twisted among the products. At the same time, the computed energy barriers (Table 9) indicate that the reaction with (+)-DSA is not characterized by the lowest energy barrier. Hence, our data suggest that the experimentally observed difference in alkylation rates between the three ligands could not be directly connected to the inter-subunit twist found in the bound conformations, in terms of induced twist in the free ligand by the DNA. In fact, an increase of the twist in **P** is not associated with a decrease in the activation energy.

**Table 9** Energy differences in kcal mol$^{-1}$ (298.15 K, 1 atm) in the gas phase [PBE0/6-31G(d)] and in aqueous solution [PCM–PBE0/6-31G(d)] for compounds **1**, **2** and **3** with adenine

| | Compound | | |
|---|---|---|---|
| Gas phase | **1** | **2** | **3** |
| $\Delta E^{\ddagger}$ (TS–reactants) | 30.9 | 29.8 | 31.1 |
| $\Delta E$ (P–reactants) | 18.1 | 18.0 | 19.8 |
| $\varepsilon = 4.0$ | | | |
| $\Delta E^{\ddagger}$ (TS–reactants) | 30.6 | 28.9 | 30.1 |
| $\varepsilon = 8.0$ | | | |
| $\Delta E^{\ddagger}$ (TS–reactants) | 30.3 | 28.5 | 29.8 |
| $\varepsilon = 78.0$ | | | |
| $\Delta E^{\ddagger}$ (TS–reactants) | 28.7 | 26.9 | 27.8 |
| $\Delta E$ (P–reactants) | 5.0 | 5.1 | 7.2 |

**Table 10** Bond lengths for the transition states of the reactions of compounds **1**, **2** and **3** with adenine optimized for the gas phase [PBE0/6-31G(d)]

| | | Bond length/Å | | |
|---|---|---|---|---|
| Bond | Nucleophile | **1** | **2** | **3** |
| C1–C10 | Adenine | 2.118 | 2.117 | 2.128 |
| C1–Nu | Adenine | 1.908 | 1.908 | 1.892 |

The most significant result concerns the electronic effect of the methyl ester group on the alkylation reaction, which becomes apparent upon comparison of the reactions of (+)-DSI and (+)-CPI with adenine. As seen above, the two systems show very similar geometric features for the reactants, transition states and products (Tables 8, 10), but the activation energy is lower for (+)-DSI than for (+)-CPI (Table 9), in full agreement with the experimental results. In terms of electronic effects, our data parallel the greater electrophilic character of (+)-DSI compared with (+)-CPI, mirroring the influence of an electron withdrawing substituent. The slightly larger positive Mulliken atomic charge on the C1 carbon is a direct answer to this effect: (+)-DSI ($q$ = +0.069) and (+)-CPI ($q$ = +0.064). At the same time, the reactivity order of the three compounds (**1**, **2**, **3**) toward adenine predicted by the donor–acceptor intermolecular hardness is in agreement with these results (*i.e.* $\eta_{DSI} \sim \eta_{DSA} < \eta_{CPI}$, see Fig. SI-3†) confirming the role of the methyl ester group on the reacting unit in increasing the ligand electrophilicity by stabilizing the LUMO. This analysis provides an explanation of the reactivity difference between DSI and CPI, which is not rationalizable in terms of geometric characteristics only.

On the other hand, some experimental studies[17] proved that (+)-DSI is less reactive than (+)-CPI under acid conditions (solvolysis). This seems in contrast with the electronic effect of the methyl ester group on the reactivity discussed above. Thus, we also decided to investigate the attack of the nucleophile to a protonated form of our model compound (Scheme 2).

The comparison of the calculated activation energies of (+)-*N*-Boc-DSA (**5**) and (+)-*N*-Boc-CPI (**4**) in acid conditions, reveals that the derivative with the ester group (**5**) is slightly more reactive (activation energy of 14.3 *vs.* 15.0 kcal mol$^{-1}$). In particular, the presence of a methyl ester group significantly reduces the negative

 

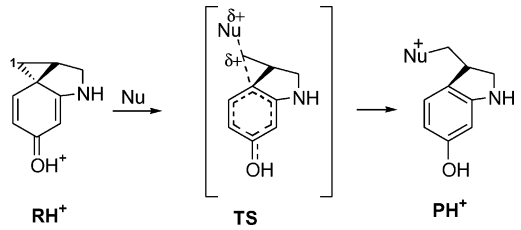


**Scheme 2** Schematic pathway for the $S_N2$ reaction, under acid conditions.

charge on the carbonyl oxygen (−0.533 *vs.* −0.550 from a Mulliken population analysis), whereas the effect on the cyclopropyl carbon is small ($q = +0.065$ *vs.* +0.060). This means that the change of the electronic distribution due to the presence of a withdrawing group on the A subunit influences substantially the basicity of the oxygen atom which, under solvolytic conditions, could be less easily protonated for (+)-DSI, with a consequently reduced reactivity. This hypothesis is confirmed by the fact that the protonation is more favorable by 1.9 kcal mol$^{-1}$ (at the PBE0/6-31G(d) level) when the methyl ester group is present.

**3.3.2 The methoxy groups on the binding unit.** Let us now compare the reaction of adenine with (+)-DSA (**1**) and (+)-DSI (**2**) (Fig. 6). On the one hand, experiments and computations agree in predicting a significantly larger torsion angle $\chi_1$ in the DSA–adenine product than in the DSI–adenine one (Table 8). However, the computed activation energy of (+)-DSA is higher than that of (+)-DSI ($\Delta E^{\ddagger} = 30.9$ kcal mol$^{-1}$ for DSA *vs.* $\Delta E^{\ddagger} = 29.8$ kcal mol$^{-1}$ for DSI), whereas on the basis of the experimental rates the natural compound (**1**) is twenty times faster than the synthetic one (**2**). Thus, in the absence of other intermolecular interactions the methoxy groups on the binding unit do not increase the reaction rate. Of course, specific interactions between the methoxy groups and suitable DNA fragments and/or water molecules structured in the minor groove could influence the activation barrier of the alkylation reaction in terms of stereo-electronic effects. Indeed, it is known that phosphate groups are principal hydration sites and that each nucleotide is closely associated with several water molecules. Analysis of several sets of experimental data, regarding the synthesis and the evaluation of the relative rates of structural analogues, leads to the conclusion that the methoxy group **M1** (Fig. 1) is essential for attaining the full alkylation activity of (+)-DSA, whereas the adjacent **M2** and **M3** methoxy groups have a negligible effect on alkylation rates.[22] In particular, elimination of **M1** reduces the alkylation efficiency by 5–20 times. Examination of the structure of the (+)-DSA complex reveals that **M1** has close contacts with some DNA fragments (thus effectively extending the length of the ligand on the side facing the minor groove), whereas **M2** and **M3** do not show any short contact with other parts of the DNA. Since the methoxy group **M1** is completely and deeply embedded in the minor groove, it can provide stabilizing non covalent binding contacts that may account, at least in part, for its dominant role in the alkylating properties of (+)-DSA.[28] We have, therefore, selected two model systems in which one and two water molecules are placed near the oxygen atom of the **M1** group with an orientation suitable to the formation of two hydrogen bonds (Fig. 7). In the gas phase, the activation energy of these models is lowered by 3.1 and 7.1 kcal mol$^{-1}$ with respect to that of the free reactants, respectively. In addition, we approximated non specific environmental effects in the minor groove by means of a polarizable continuum with a dielectric constant of 4.0, obtaining a further reduction of the energy barrier of about 1 kcal mol$^{-1}$. In summary, a model including specific fragments surrounding the ligand together with non specific environmental effects is able to reduce the activation energy of (+)-DSA to below that of (+)-DSI. Thus, electronic effects of DNA residues close to the methoxy groups cannot be neglected for a satisfactory explanation of the DNA catalytic mechanism, with the hydrogen bonds formed by the **M1** oxygen playing the most significant role. In order to analyze the origin of this stereo-electronic effect we resorted again to reactivity indexes: the decrease of the intermolecular hardness ($\eta_{DA}$) between (+)-DSA and adenine (7.42 eV and 7.33 eV with one and two water molecules, respectively) below that of (+)-DSI (7.47 eV) again points out the role of polarization effects in stabilizing the ligand LUMO with the consequent increase of electrophilicity and reactivity.

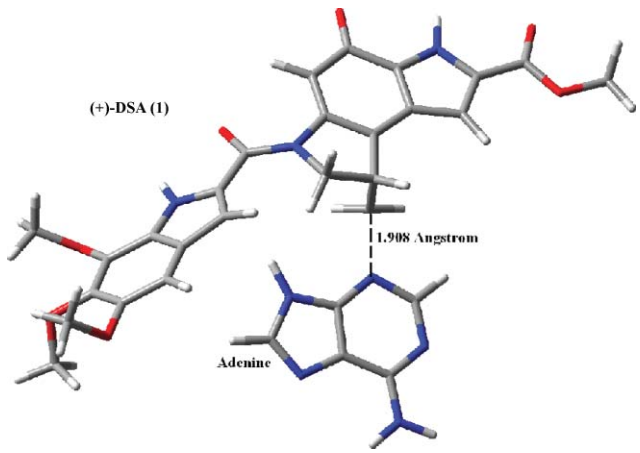


**Fig. 6** Structure of the transition state of **1** with adenine optimized at PBE0/6-31G(d) level.

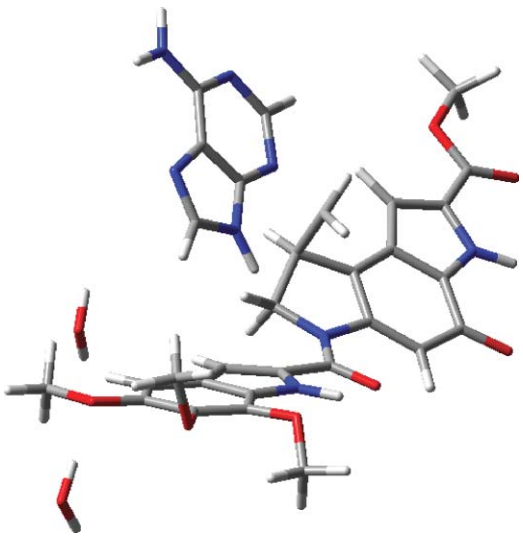

**Fig. 7** Structure of the transition state of (+)-DSA with adenine with 2 water molecules.

As a last point, let us underline that intermolecular interactions could "lock" the ligand into the minor groove, leading

from an intermolecular reaction (bimolecular in solution) to an intramolecular one (first-order in DNA), where the rate enhancement is related to the formation of some sort of pre-complex. The rate increase when a bimolecular reaction is converted into a unimolecular one is related to the entropy change when translational and rotational motions of reactants in a bimolecular reaction are transformed into low-frequency vibrations of the pre-complex.

## 4. Conclusions

The application of an integrated computational approach has provided, in our opinion, some interesting results about the role of stereo-electronic effects in tuning the DNA alkylation process by (+)-DSA. The most significant aspects can be summarized as follows:

1. As already found in previous computations[24] and in agreement with experimental evidence, our calculations indicate that the cyclopropane ring-opening of compounds **1**, **2** and **3**, upon nucleophilic attack of adenine at the least substituted carbon atom (C1) follows the $S_N2$ mechanism.

2. The computed activation energy governing the reaction of (+)-DSA with guanine is about 8 kcal $mol^{-1}$ higher than for the reaction with adenine. Although different steric accessibilities can, of course, lead to selective alkylation of adenine, our results suggest that local stereo-electronic effects also play a significant role.

3. Specific hydrogen bond interactions reduce the activation energy of the title reaction, which becomes feasible under neutral conditions also. Moreover, specific non-covalent interactions between the ligand and sites that are located in the DNA minor groove play a significant role in determining the rate enhancement experimentally observed in DNA with respect to the corresponding process in solution.

4. The electron-withdrawing methyl ester substituent, bonded to the alkylating subunit of (+)-DSA, promotes the nucleophilic attack and, by increasing the positive charge on the reactive cyclopropyl carbon, decreases the activation energy leading, in agreement with the experiments, to a faster alkylation with (+)-DSI than with (+)-CPI.

5. Specific interactions between the methoxy groups on the binding subunit and the DNA environment decrease the activation energy governing the alkylation process of (+)-DSA below that of the corresponding reaction with (+)-DSI. Once again stereo-electronic effects play a role in determining the experimentally observed trend of reaction rates.

6. According to our results, the inter-subunit twist plays a marginal role in tuning DNA alkylation rates. As a matter of fact, modifications of the key dihedral angles ($\chi_1$, $\chi_2$ and $\chi_3$) as large as 20° change the activation energy by less than 1 kcal $mol^{-1}$ from a reference value of ≈30 kcal $mol^{-1}$.

In conclusion, we think that our results provide some interesting hints about the interplay of different effects in determining the overall outcome of duocarmycin alkylation. Furthermore, together with the intrinsic interest of the investigated system, the present study confirms, in our opinion, that an integrated computational tool, rooted in density functional theory and continuum solvent models, offers a valuable aid toward the elucidation of the role of different effects involved in processes of biological and pharmacological interest.


## Acknowledgements

The authors thank the Italian Ministry of University and Research (MIUR) for financial support and the Campus Grid at the University Federico II for computer facilities.


## References


1 M. Demeunynck, C. Bailly and W. D. Wilson, *Small Molecule DNA and RNA Binders*, Wiley-VCH, Darmstadt, 2003.
2 R. Martinez and L. Chacon-Garcia, *Curr. Med. Chem.*, 2005, **12**, 127–151.
3 C. J. Suckling, *Expert Opin. Ther. Pat.*, 2004, **14**, 1693–1724.
4 M. H. David-Cordonnier, W. Laine, T. Gaslonde, S. Michel, F. Tillequin, M. Koch, S. Leonce, A. Pierre and C. Bailly, *Curr. Med. Chem.: Anti-Cancer Agents*, 2004, **4**, 83–92.
5 G. J. Anne, T. Furuta and Y. Pommier, *Anti-Cancer Drugs*, 2002, **13**, 545–562.
6 P. Cozzi, *Farmaco*, 2001, **56**, 57–65.
7 C. Geroni, S. Marchini, P. Cozzi, E. Galliera, E. Ragg, T. Colombo, R. Battaglia, M. Howard, M. D'Incalci and M. Broggini, *Cancer Res.*, 2002, **62**, 2332–2336.
8 S. C. Wilson, P. W. Howard, S. M. Forrow, J. A. Hartley, L. J. Adams, T. C. Jenkins, L. R. Kelland and D. E. Thurston, *J. Med. Chem.*, 1999, **42**, 4028–4041.
9 S. J. Gregson, P. W. Howard, J. A. Hartley, N. A. Brooks, L. J. Adams, T. C. Jenkins, L. R. Kelland and D. E. Thurston, *J. Med. Chem.*, 2001, **44**, 737–748.
10 S. E. Wolkenberg and D. L. Boger, *Chem. Rev.*, 2002, **102**, 2477–2496.
11 D. L. Boger and D. L. Johnson, *Angew. Chem., Int. Ed. Engl.*, 1996, **35**, 1438–1474.
12 D. L. Boger, D. L. Hertzog, B. Bollinger, D. L. Johnson, H. Cai, J. Goldberg and P. Turnbull, *J. Am. Chem. Soc.*, 1997, **119**, 4977–4986.
13 D. L. Boger, B. Bollinger, D. L. Hertzog, D. L. Johnson, H. Cai, P. Mesini, R. M. Garbaccio, Q. Jin and P. A. Kitos, *J. Am. Chem. Soc.*, 1997, **119**, 4987–4998.
14 S. Nagamura, A. Asai, E. Kobayashi, K. Gomi and H. Saito, *Bioorg. Med. Chem.*, 1997, **5**, 623–630.
15 N. Amishiro, S. Nagamura, E. Kobayashi, A. Okamoto, K. Gomi, M. Okabe and H. Saito, *Bioorg. Med. Chem.*, 2000, **8**, 1637–1643.
16 P. G. Baraldi, G. Balboni, M. G. Pavani, G. Spalluto, M. A. Tabrizi, E. De Clercq, J. Balzarini, T. Bando, H. Sugiyama and R. Romagnoli, *J. Med. Chem.*, 2001, **44**, 2536–2543.
17 A. Sato, L. McNulty, K. Cox, S. Kim, A. Scott, K. Daniell, K. Summerville, C. Price, S. Hudson, K. Kiakos, J. A. Hartley, T. Asao and M. Lee, *J. Med. Chem.*, 2005, **48**, 3903–3918.
18 D. L. Boger, R. J. Wysocki, Jr. and T. Ishizaki, *J. Am. Chem. Soc.*, 1990, **112**, 5230–5240.
19 D. L. Boger and P. Mesini, *J. Am. Chem. Soc.*, 1994, **116**, 11335–11348.
20 D. L. Boger, J. A. Goldberg and A. McKie, *Bioorg. Med. Chem. Lett.*, 1996, **6**, 1955–1960.
21 D. L. Boger, A. Santillan, Jr., M. Searcey and Q. Jin, *J. Org. Chem.*, 1999, **64**, 5241–5244.
22 D. L. Boger, C. W. Boyce and D. L. Johnson, *Bioorg. Med. Chem. Lett.*, 1997, **7**, 233–238.
23 D. L. Boger and R. M. Garbaccio, *J. Org. Chem.*, 1999, **64**, 5666–5669.
24 Y. Ambroise and D. L. Boger, *Bioorg. Med. Chem. Lett.*, 2002, **12**, 303–306.
25 D. L. Boger, A. Santillan, Jr., M. Searcey and Q. Jin, *J. Am. Chem. Soc.*, 1998, **120**, 11554–11557.
26 D. L. Boger and R. M. Garbaccio, *Acc. Chem. Res.*, 1999, **32**, 1043–1052.
27 D. L. Boger, D. S. Johnson and W. Yun, *Bioorg. Med. Chem. Lett.*, 1994, **116**, 1635–1656.
28 D. L. Boger, B. Bolliger and D. S. Johnson, *Bioorg. Med. Chem. Lett.*, 1996, **6**, 1955–1960.
29 R. S. Coleman and D. L. Boger, in *Studies in Natural Products Chemistry, vol. 3*, ed. A.-U. Rahman, Elsevier, Amsterdam, 1989, pp. 301–309.
30 W. Kock and W. C. Holthousen, *A Chemist's Guide to Density Functional Theory*, Wiley-VCH, Weinheim, 2000.
31 C. Adamo, M. Cossi, N. Rega and V. Barone, in *Theoretical Biochemistry: Processes and Properties of Biological Systems. Theoretical*


 

*and Computational Chemistry*, Elsevier, New York, 2001, vol. 9, pp. 467–538.
32 M. Cossi, N. Rega, G. Scalmani and V. Barone, *J. Chem. Phys.*, 2002, **117**, 43–54.
33 C. Adamo and V. Barone, *J. Chem. Phys.*, 1999, **110**, 6158–6170.
34 M. J. Frisch, G. W. Trucks, H. B. Schlegel, G. E. Scuseria, M. A. Robb, J. R. Cheeseman, J. A. Montgomery, Jr., T. Vreven, K. N. Kudin, J. C. Burant, J. M. Millam, S. S. Iyengar, J. Tomasi, V. Barone, B. Mennucci, M. Cossi, G. Scalmani, N. Rega, G. A. Petersson, H. Nakatsuji, M. Hada, M. Ehara, K. Toyota, R. Fukuda, J. Hasegawa, M. Ishida, T. Nakajima, Y. Honda, O. Kitao, H. Nakai, M. Klene, X. Li, J. E. Knox, H. P. Hratchian, J. B. Cross, V. Bakken, C. Adamo, J. Jaramillo, R. Gomperts, R. E. Stratmann, O. Yazyev, A. J. Austin, R. Cammi, C. Pomelli, J. Ochterski, P. Y. Ayala, K. Morokuma, G. A. Voth, P. Salvador, J. J. Dannenberg, V. G. Zakrzewski, S. Dapprich, A. D. Daniels, M. C. Strain, O. Farkas, D. K. Malick, A. D. Rabuck, K. Raghavachari, J. B. Foresman, J. V. Ortiz, Q. Cui, A. G. Baboul, S. Clifford, J. Cioslowski, B. B. Stefanov, G. Liu, A. Liashenko, P. Piskorz, I. Komaromi, R. L. Martin, D. J. Fox, T. Keith, M. A. Al-Laham, C. Y. Peng, A. Nanayakkara, M. Challacombe, P. M. W. Gill, B. G. Johnson, W. Chen, M. W. Wong, C. Gonzalez and J. A. Pople, *GAUSSIAN 03 (Revision C.02)*, Gaussian, Inc., Wallingford, CT, 2004.
35 A description of basis sets and standard computational methods can be found in: J. B. Foresman and A. E. Frisch, *Exploring Chemistry with Electronic Structure Methods*, Gaussian, Inc., Pittsburg, PA, 2nd edn, 1996.
36 (*a*) J. Tomasi and M. Persico, *Chem. Rev.*, 1994, **94**, 2027–2094; (*b*) J. Tomasi, B. Mennuci and R. Cammi, *Chem. Rev.*, 2005, **105**, 2999–3094.
37 C. Gonzalez and H. B. Schlegel, *J. Phys. Chem.*, 1990, **16**, 1170–1176.
38 A. E. Reed, L. A. Curtiss and F. Weinhold, *Chem. Rev.*, 1988, **88**, 899–926.
39 R. Parr and R. G. Pearson, *J. Am. Chem. Soc.*, 1983, **105**, 7512–7516.
40 R. G. Pearson, *Chemical Hardness*, 1997, VCH, Weinheim.
41 I. Ciofini, S. Hazebroucq, L. Joubert and C. Adamo, *Theor. Chem. Acc.*, 2004, **111**, 188–195.
42 R. G. Parr, L. Szentpaly and S. Liu, *J. Am. Chem. Soc.*, 1999, **121**, 1922–1924.
43 H. Chermette, *J. Comput. Chem.*, 1999, **20**, 129–154.
44 D. G. Martin, R. C. Kelly, W. Watt, N. Wicnienski, J. W. Mizsak, W. J. Nielsen and M. D. Prairie, *J. Org. Chem.*, 1988, **53**, 4610–4613.
45 D. L. Boger, A. Santillan, Jr., M. Searcey, S. R. Brunette, S. E. Wolkenberg, M. P. Hedrick and Q. Jin, *J. Org. Chem.*, 2000, **65**, 4101–4111.
46 P. S. Eis, J. A. Smith, J. M. Rydzewski, D. A. Case, D. L. Boger and W. J. Chazin, *J. Mol. Biol.*, 1997, **272**, 237–252.
47 J. A. Smith, G. Bifulco, D. A. Case, D. L. Boger, L. Gomez-Paloma and W. J. Chazin, *J. Mol. Biol.*, 2000, **300**, 1195–1204.
48 J. R. Schnell, R. R. Ketchem, D. L. Boger and W. J. Chazin, *J. Am. Chem. Soc.*, 1999, **121**, 5645–5652.
49 C. Bassarello, P. Cimino, G. Bifulco, D. L. Boger, J. A. Smith, W. J. Chazin and L. Gomez-Paloma, *ChemBioChem*, 2003, **4**, 1188–1193.
50 P. Cimino, R. Improta, G. Bifulco, R. Riccio, L. Gomez-Paloma and V. Barone, *J. Org. Chem.*, 2004, **69**, 2816–2824.
51 P. Cimino, L. Gomez-Paloma and V. Barone, *J. Org. Chem.*, 2004, **69**, 7414–7422.
52 G. S. Hammond, *J. Am. Chem. Soc.*, 1955, **77**, 334–338.
53 N. Rega, S. S. Iyengar, G. A. Vogt, H. B. Schlegel, T. Vreven and M. J. Frisch, *J. Phys. Chem. B*, 2004, **108**, 4210–4220.
54 S. Tanizaki and M. Feig, *J. Chem. Phys.*, 2005, **122**, 124706.
55 V. Barone, R. Improta and N. Rega, *Theor.Chem. Acc.*, 2004, **111**, 237–245.
56 K. N. Kirschner, M. Lee, R. Stanley and J. P. Bowen, *Bioorg. Med. Chem.*, 2000, **8**, 329–335.